Design of a Narrow Band Hydrogen-Alpha Astrophotography Filter Based on One Dimensional Photonic Crystals

ASHLEY KIM,[1]

Korea International School, 27, Daewangpangyo-ro, 385 beon-gil Bundang-gu, Seongnam-si, Gyeonggi-do South Korea

[*]*ashley.lc.kim@gmail.com*

Abstract:

Several astrophotography filters are currently used to isolate the targeted wavelength of H-alpha, O3, and H-beta for a clearer capture of nebulae; however they fail to achieve both highest possible transmittance and low focus band width. This paper presents a novel nebula filter incorporating three 1-dimensional photonic crystal created through deposited layers of TiO2 and SiO2. The design was able to achieve 97.9 percent transmittance rate in 656.3 nm wavelength of H-alpha, as well as Full Width at Half Max (FWHM) of mere 0.1 nm, while blocking almost every other wavelength of the visible light spectrum. This filter design is a clear improvement from any other currently existing products and shows high applicability due to its relatively uncomplicated depositing structure and its flexibility from the possible algorithmic manipulation of the targeted wavelengths.

1. Introduction

Astronomy, a study of our universe and its celestial bodies, without a doubt relies on the capture and analysis of electromagnetic radiation [1]. Our perception and study of the universe beyond comes from data and photographs collected through means such as advanced telescopes or cameras. However, as millions of light years separate the Earth and those objects, capturing and visibly representing the emitted lights comes with great difficulties. Solely photographing the whole spectrum of electromagnetic wave fails to illustrate our universe to its fullest, as different characteristics and components of the universe are revealed at different wavelengths. Some objects are completely invisible at one wavelength yet are clearly visible at another [2]. Thus, it is natural that techniques and means for conducting the isolated capture of certain wavelengths of electromagnetic waves becomes a central focus in advancing the study of outer space and beyond.

Especially in astrophotography, the need for isolated focus of some wavelengths comes from several reasons. First, as the capture of light happens on Earth, it is critical that the resulting photograph is not contaminated or blurred by light pollution and light from any extraneous sources. Next, some elements or electromagnetic waves are specific to certain types of celestial bodies and require focus to produce a more clearer product. For instance, for emission nebulae, nebula formed of ionized gases and consisting of around 90% hydrogen, most of light emitted is consists of wavelengths of Hydrogen Alpha (H-Alpha or H_α) at 656.279 nm [3]. This type of nebulae are called HII regions, and has its distinctive red color due to this overwhelming emission of H-Alpha wavelengths [4]. Hydrogen Beta is another type of light that is emitted by these nebulae. While the emission is small compared to that of H-Alpha, H-Beta has the wavelength of 486.135 which is represented by a bright blue color [5]. On the other hand, for planetary nebulae - a type of emission nebula consisting of expanding shells of ionized gas [6] - O^2+ (or namely, OIII) of 500.7 nm wavelength distinctively marks its visible emission [7]. Thus, photographing such nebulae is better achieved through focusing on the capture of these specific light wavelengths. In astrophotography, this is achieved through optical filters that aim to filter out every other wavelengths of the spectrum except the targeted wavelength. An example is

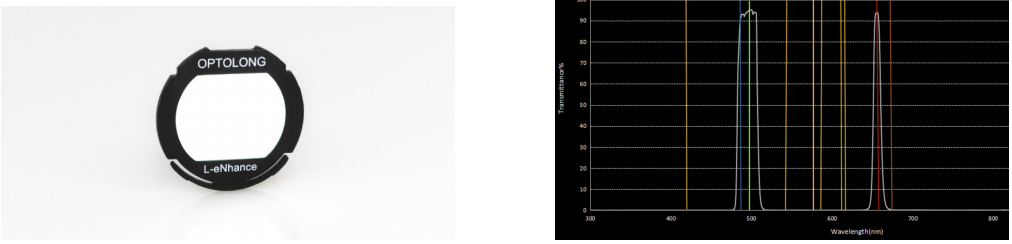

(a) Picture.

(b) Transmittance Spectra.

Fig. 1. L-eNhance EOS-C Filter and its Transmittance Spectra.
[10]

the H-Alpha dichroic filters, which are deemed essential for imaging nebulae and other objects which are rich in ionized hydrogen [8]. These dichroic filters block the propagation of other wavelengths except the narrow band centered at 656.279 nm of H-Alpha.

Currently, a multitude of products exists; some filters isolate the wavelength of H-Alpha, B-Beta, OIII, or take in multiples combination them [9]. These filters block wavelengths of light of natural light caused by neutral oxygen emission in our atmosphere, or unwanted elements such as Sodium and Sulfur. However, a problem exists across all currently produced filters, as they are unable to achieve the maximum focus and efficiency. For instance, while a filter shown in Figure 1 is able to isolate the H-Alpha, H-Beta, and O_3 from every other wavelength, it is only able to achieve a transmittance rate of around 93% [10]. If a filter were able to achieve a high propagation rate of up to 95%, this would result in a very inefficient focus on the targeted wavelengths, such as a band width of up over 40 nm [8]. A product was able to isolate 3 different, specific wavelengths in a single filter with band width of 3 nm, but the percentage of transmittance only amounted for 85% [11]. While the difference from 100% is only 5 to 15%, it has significant implications in the case of astrophotography or capturing a celestial body located an unimaginable distance away. The 5% increase in transmittance can reveal an unknown component, history, and object around and about these nebula, and considering the increasing light pollution and atmospheric distortion, an improvement in the filters' transmittance rate and focus is essential.

This research proposes a novel design of nebulae dichroic optical filter with the Photonic Crystal nanostructure. Utilizing the unique characteristics of the photonic crystal band gap and its defect modes, we were successful in developing a structure that allowed for 100% transmittance rate of targeted wavelength centered at 656.3 nm (H-alpha). Furthermore, the filter was able to isolate the wavelength with a focus band width down to less than 1 nm. Each of the 3 photonic crystals composing the whole filter system was composed with TiO2 and SiO2 material. Its capacity is an improvement of transmittance rate up to 97.9% better than any other currently existing dichroic filters, and promises a very high focus on the targeted wavelength.

2. Photonic Crystals Theory

2.1. Fundamentals of Photonic Crystal Design and Band Gaps

The Photonic Crystal is an optical nanostructure that contains periodic variations of the refractive index [12]. Its unique composition and structure give rise to its optical characteristics, mainly the ability to control the propagation of different wavelengths of electromagnetic light [13]. The concept of a photonic crystal was first clearly described by Yablonovitch, who suggested that structures composed of high and low refraction index materials could lead to allowed or forbidden propagation of certain electromagnetic frequencies in a manner very similar to the way

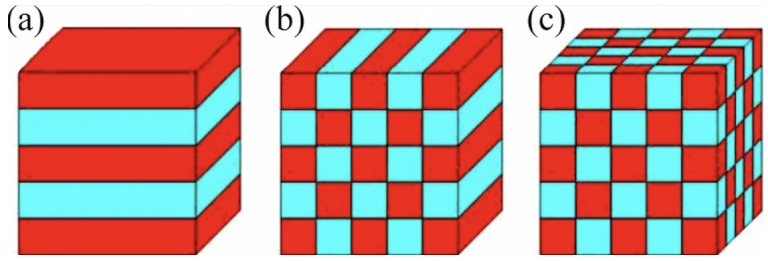

Fig. 2. 1D, 2D, 3D Photonic Crystal Structures.
[12]

in which a lattice of atoms give rise to allowed and forbidden electron energies [14]. For certain frequencies or wavelengths of light, photonic crystals prevent its propagation in any direction within the material. This certain "gap," or range in wavelength, is named the photonic crystal band gap, due to its similar properties with the electronic band gap of semiconductors [15]. The photonic crystal band gaps are understood as the destructive interference of multiple reflections of light propagating in the crystal at each interface between layers of high and low refractive index regions of the structure, akin to the band gaps of electrons in solids [16]. In other words, photonic crystals can be analogous to filters of light, allowing the control of transmittance of certain ranges of the spectrum through the medium. This unique optical characteristic of the photonic crystal band gap promises various applications in fields of material science, optical fibers and filters, bio sensing, and more [17] [18].

Photonic crystal structures frequently arise in nature, in forms of brightly colored wings, feathers, and exoskeletons of organisms, and are composed of a complex mixture of biopolymeric compounds and proteins [19]. However they can also be manufactured artificially, in forms of one (1D), two (2D), and three (3D) dimensional crystal structures, as shown in Figure 2. One dimensional photonic crystals can be manufactured by periodically and alternatively depositing thin film layers of different dielectric constants on a surface which leads to a band gap in a particular propagation direction, such as normal to the depositing surface [20]. The alternating structure is demonstrated through Figure 3, with n_1 and n_2 being the high and low refractive index of the incorporated two materials. Meta-materials and vacuum can also be utilized as alternating layers to design purposeful band gaps [21]. 2D and 3D photonic crystals can be engineered by drilling holes into substrates with particular optical characteristics, or through structures such as wood pile rods [22]. Due to the limitations of current fabrication technology, 2D and higher level photonic crystals are yet to be applied in powerful applications, and research on more efficient, successful engineering methods is ongoing.

The band gap of photonic crystals can be manipulated through various factors such as the refractive index and width of the materials, as well as the system and periodicity of the alternating layers. The abundance of materials with different refractive indices and the possibilities of combinations in the width and depositing sequence signal the great magnitude of number of possible unique structures and resulting band gaps, even in more simplistic designs of 1D crystal structures. This research will focus primarily on the engineering of 1D photonic crystal structures, in which more accurate prototyping and calculations are possible.

2.2. Transfer Matrix Method (TMM) Calculation

The Transfer Matrix Method [23] is a method used in optics to analyze the propagation of electromagnetic waves through multi-layer of thin films of different material. It consists of writing the Maxwell's equations in the k-space and rewriting them, performing the operation with layer-by-layer calculations [23]. The photonic crystal's band structure, reflectivity, and transmission

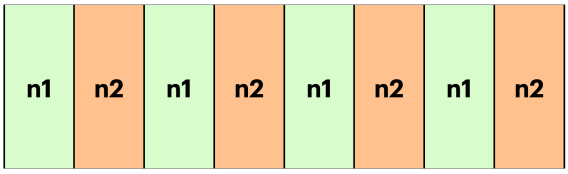

Fig. 3. Schematic of 1D Photonic Crystal structure.

coefficients can be easily found with this method. In the case of photonic crystals, TMM is used to graph the reflectance and transmittance spectra through the range of electromagnetic wavelengths, and to graph the location, width, and other components of the band gap.

A plane wave normally propagating through a layered medium undergoes reflections and transmissions at the layer boundaries, which in turn undergo their own reflections and transmissions in an unending process [24]. The amplitudes of the transmitted and reflected waves can be determined at each boundary. Thus the overall transmittance and reflectance of a medium can, in principle, be calculated by multiplication of these individual waves. The tracking of the complex amplitudes of the forward and backward waves through the boundaries of a multilayered medium is facilitated by use of matrix methods. Consider an arbitrary plane in a given optical system, with the amplitudes of the forward and backwards waves denoted by U^+ and U^-, respectively [24]. The plane and the propagating rays are demonstrated above in Figure 4. These waves are ultimately represented by a column matrix of dimension 2.

$$\begin{bmatrix} U_2+ \\ U_2- \end{bmatrix} = \begin{bmatrix} A & B \\ C & D \end{bmatrix} \begin{bmatrix} U_1+ \\ U_1- \end{bmatrix} \tag{1}$$

The matrix M as described in Equation 1 is the 2 by 2 matrix with elements A, B, C, and D, and it is called the wave-transfer matrix (or transmission matrix). Its values depend on the optical properties of the layered medium between the two planes [24]. A multilayered medium is conveniently translated into a sequence of these transmission matrices with basic elements, known as wave-transfer matrices, following the direction of movement of the wave through the medium. The amplitudes of the forward and backward collected waves at the two ends of the overall medium are then represented by a single matrix that is the matrix product of the individual wave-transfer matrices. Thus, the objective and process of the Transfer Matrix Methods comes down to calculating the individual wave-transfer matrix of propagation of each layer, and performing matrix multiplication of all to find the reflectance and transmittance of the overall medium.

The individual wave-transfer matrices can be further broken down to 2 components, the propagation and the boundary. The propagation matrix represents the propagation of the electromagnetic wave through a homogeneous medium, or in the case of the photonic crystal structure, through the single layer of one material. Equation 2 notes the general matrix formula for each propagation matrices, for a homogeneous layer with width d and refractive index of n. k_o is equal to $\frac{2\pi}{lambda}$, with lambda being the specific wavelength value for the TMM to calculate the reflection and transmittance value of.

$$M = \begin{bmatrix} exp(-j\varphi) & 0 \\ 0 & exp(j\varphi) \end{bmatrix}, \varphi = nk_o d \tag{2}$$

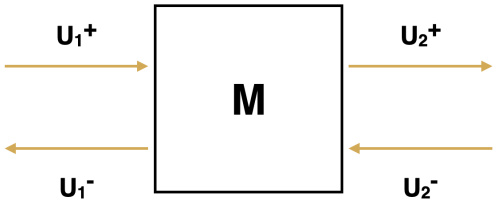

Fig. 4. Demonstration of M Matrix and Propagating Waves.

The boundary matrix for the transmittance and reflectance at a boundary between two media of refractive indices n_1 and n_2 is indicated by the Equation 3.

$$M = \frac{1}{2n_2}\begin{bmatrix} n_2 + n_1 & n_2 - n_1 \\ n_2 - n_1 & n_2 + n_1 \end{bmatrix} \tag{3}$$

After matrix multiplication of the propagation and boundary matrices of all layers, the resulting TMM will be represented as Equation 4 with t and r yield 2 complex numbers standing for transmission and reflection.

$$M = \begin{bmatrix} -1/t & r/t \\ -r/t & 1/t \end{bmatrix} \tag{4}$$

Thus we can calculate the real values by squaring the absolute value of those 2 variables, and ultimately graphing the transmittance and reflection of the photonic crystal over a range of wavelengths by inserting the different wavelength values into the lambda of the propagation matrix. Figure 5 is the spectra graph using the TMM calculation method, graphed through python code. It demonstrates the propagation pattern of a photonic crystal composed of 10 layers of SiO_2 and TiO_2 with refractive index value of approximately 1.5 and 2.5 respectively, drawn over a lambda range from 400 to 800 nm. The photonic crystal band gap is evident from the graph, as shown by the range from approximately 520 to 720 nm with 1.0 out of 1.0 percent reflectance, illustrating the wavelength ranges where propagation through is prohibited by the photonic crystal.

2.3. Band Gap and Defect Mode Engineering

The photonic crystal band gap can be purposefully manipulated through the change in the optical characteristics of the layers, such as the refractive index, thickness, and the system of disposition. Furthermore, another fundamental component related to photonic crystal is defect modes within the structure. The defect modes are generally generated when the translational symmetry in a crystal is broken [25], which can be done by inserting a defect layer into the crystal or removing a single layer from the structure. Similar to the band gaps, the creation and characteristics of the defect mode is very dependent on the structure, materials and thickness of the considered photonic crystal. This section will demonstrate several methods in effectively manipulating and engineering the band gaps and defect modes.

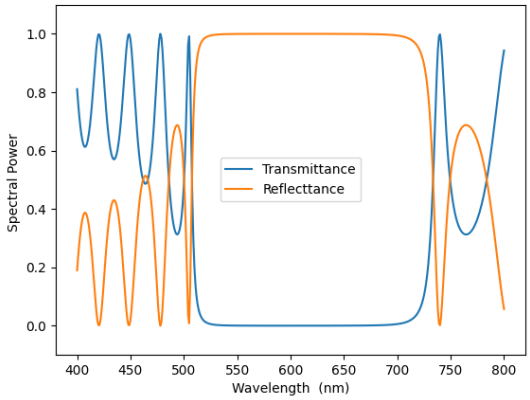

Fig. 5. Spectra Graph of Reference 1D Photonic Crystal.

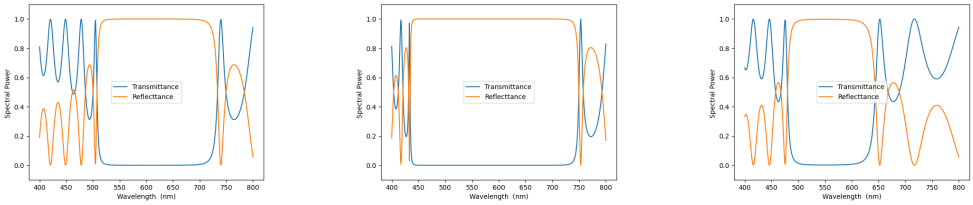

(a) Δn = 1.0. (b) Δn = 1.5. (c) Δn = 0.7.

Fig. 6. Effect of Bigger Refractive Index Difference in Band Gap.

2.3.1. Refractive Index Difference

Given a 1D photonic crystal composed of 2 materials with different refractive indices, repeatedly disposed 10 times each with identical thickness, the width of the photonic band gap is directly proportional to the absolute value of the difference between the 2 refractive index. Bigger index differences result in a bigger band gap, as demonstrated through the comparison established by Figure 6a and Figure 6b. This case only analyzed when $n_1 < n_2$, but it should also be noted that only the absolute value of the difference can influence the band gap. Figure 6c demonstrates the opposite case, of smaller refractive index difference, and how it results in a smaller band gap. However, it seems like there is a minimum value of Δn such that a band gap itself can form. If Δn decreases under 0.6, while the spectra resemble the shape of a gap, reflection does not reach exactly 100 percent.

2.3.2. Thickness

The thickness of each material layer can be manipulated by changing the lambda value in the equation $d = lambda/4/n$, with d being the thickness of the layers of the material with refractive index of n. The average value of $d1$ and $d2$ of each material 1 and 2 determines the center of the band gap, as demonstrated by Figure 7b and Figure 7c. This means the band gap can be located further left or right depending on manipulation of $d1$ and $d2$. Smaller average lambda values of $d1$ and $d2$ moves the gap to the left, and larger to the right. Their effect on the width of the gap needs further investigation, as it seems like the trend is not universal.

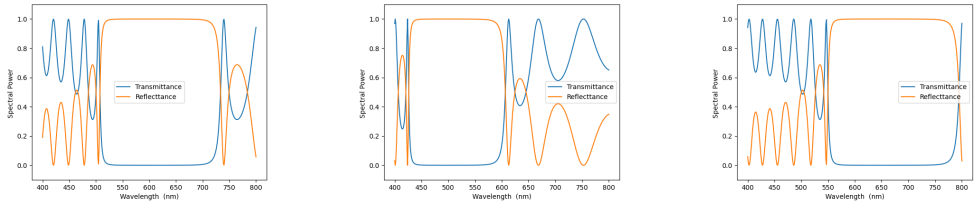

(a) Average Lambda Value = 600. (b) Average Lambda Value = 500. (c) Average Lambda Value = 650.

Fig. 7. Effect of Average Lambda Value of Thickness in Band Gap.

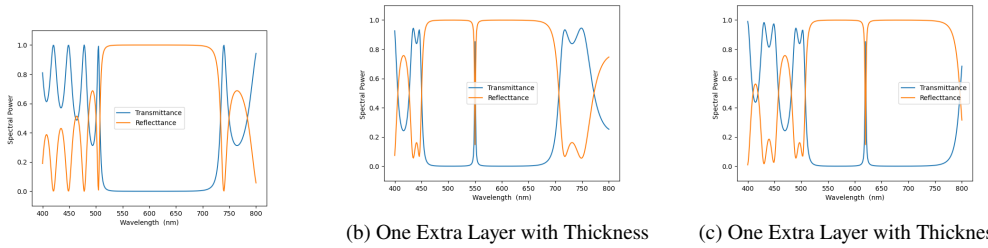

(a) No Defect. (b) One Extra Layer with Thickness Average lambda value = 550. (c) One Extra Layer with Thickness Average lambda value = 620.

Fig. 8. Defect Mode Engineering with One Extra Layer.

2.3.3. Creation of Defect Modes with extra layer

As mentioned before, defect modes can be created by inserting a defect layer into the crystal or removing a single layer from the structure and destroying the translation symmetry of the structure. Figure 8b demonstrates the defect mode created at 550 nm and 620 nm respectively. This was done by inserting an additional TiO_2 layer between the two 5 sets of layers (it can also be notated by $(LH)^5$ / H / $(LH)^5$ with L and H being the 2 layers of material). As also shown by the comparison of Figure 8b and Figure 8c, the average lambda value of the thickness also plays a role in determining the location of the defect mode. This signals that both the band gap itself and the defect mode within can be engineered by manipulating with the thickness of the two materials. More defect modes can be created in different places by inserting additional layers or complicating the insert sequence. Band gap and defect modes are a unique component of photonic crystals and appropriate engineering with the methods demonstrated above can lead to powerful application of this optical material in the real world.

3. Similar works

3.1. Single Peak Narrowband Reflection Filter Possessing Broad Low Reflecting Bypass Belt

This Single Peak Narrowband Reflection Filter with Broad Low Reflecting Bypass Belt [26] is a design submitted to the Chinese patent office. It details a photonic crystal design that is a single peak narrowband filter with a easily movable peak, and can be produced with simple preparation process. It cites optical instrument, astronomy, remote sensing and optical communications as the invention's application prospect fields.

First, the article lays out the types of the existing background technology. It cites filters based on the optical thin film of full medium, and filters based on the optical filter of sub-wavelength wave guide optical grating as the two main existing products. For the first type of thin film of full

medium, the author states that the design contains one significant problem of low transmittance rate of 30%, and a bandwidth of 10 nm after transfer optimization. Furthermore, for the second design, the author cites technology and the cost of preparation as its major limitation, arguing that its complex and expensive manufacturing process limits the use of this type of filter to only high-end research and applications. The submitter of this patent goes on to argue that this submitted design is able to counteract all of the aforementioned technological and cost-related limitations.

The proposed photonic crystal design is a medium-metal composite film system based on asymmetric Fabry-Perot structure, obtained by an improvement on the basis of standard Fabry-Perot structure. Standard Fabry-Perot structure is a type of interlayer symmetrical structure, utilizing the fact that if several cycles in a side of wall is increased or reduced, both sides of the wall lose the symmetry and produces the asymmetric Fabry-Perot structure. A metal level is superposed between the designed asymmetric Fabry-Perot structure. From there, the absorption characteristic of particulate metal layer is utilized to achieve the high transfer of the broadband and limit the width of the band. This consequently produced the high transmittance narrow band effect of the filter. The particulate metal here refers in particular to the high-absorbing metals, such as tungsten, chromium, iron, nickel, lead, or rhodium. However it can also can be other high-absorbing metals, for example the Cr metal that satisfy all the other aforementioned requirements.

The films structure itself is $Sub|(HL)^{M1}H\alpha L(HL)^{M2}\beta MP|Air$, as shown in Figure 9a. The H, L are respectively the high and low refractive index material of 1/4 wavelength optical thickness that can be engineered based on the targeted wavelength. One commonly used combination of film material with differing refractive index is TiO_2 as the high index (H), and SiO_2 as the low index layer (L). However, these two kinds of films also can be made of the metal-based materials, such as ZnS and MgF where ZnS is a high-index material, and MgF the low-index material. Sub represents the substrate of optical thin film, with refractive index is taken of 1.52. Air represents air, with refractive index of 1. In the αL layer, L is wall or defect layer, and α is the thickness coefficient of that particular wall. M is a metal level, and β is a metal layer thickness with the unit of nm. Admittance matching layer P in the described film structure can be a high-index material mono-film system, $P = \gamma H$, where γ is the thickness coefficient of H layer. Furthermore, in the listed layers, $m1$ and $m2$ are the number of repetitions of the (HL) layer. The thickness coefficient α can regulate and control the position of reflection peak, and physical thickness β is used for controlling the degree of depth of ending of reflectance spectrum. These variables can be manipulated to create different filters with narrowband peaks in different positions and magnitudes, as shown in Figure 9b and 9c.

The article also describes the simplified preparation or engineering method for the filter: (1) First, determine the film structure of $Sub|(HL)^{M1}H\alpha L(HL)^{M2}\beta MP|Air$. (2) Determine the narrowband centre wavelength according to the reflection peak position, approximate $m1$, $m2$, α, β and the thickness of the coupling film coefficient γ of P, and calculate the reflectance spectrum. (3) Optimize the matching film thickness coefficient γ of P; (4) Optimize the β parameter to achieve the desired low reflecting bypass belt degree of depth. (5) Determine $m2$ to achieve desired half width; (6) Determine α parameter so that the reflection peak is adjusted to the target location. (7) Determine $m1$ parameter to achieve high narrowband reflection. (8) Repeat step (3) to (7) are until reaching set design object. It should be noted that the above mentioned steps (3), (4) and (6) all can be finely tuned by computer technology and pre-programmed processes.

A few problems can be identified for this specific design. Firstly, the layer structure of the photonic crystal is very complex; although the authors have claimed that it simplifies the preparation process in comparison to the existing designs, a better, simpler structure should be possible. Second, similar to the products mentioned in the introduction, its transfer rate only amounts to 90%, as shown in Figure 10. A greater transfer rate, and an improvement in its focus

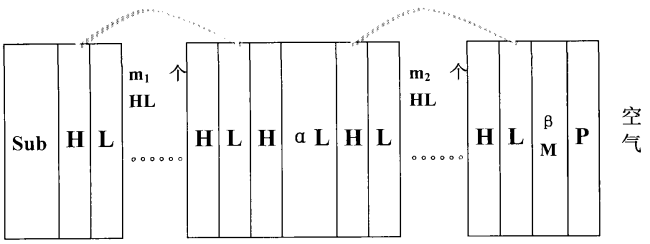

(a) Physical Layout.

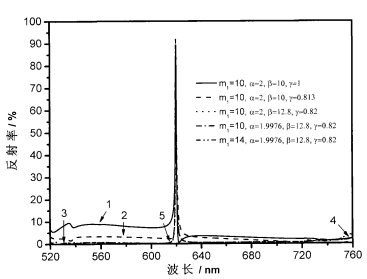

(b) Manipulation of $m1$.

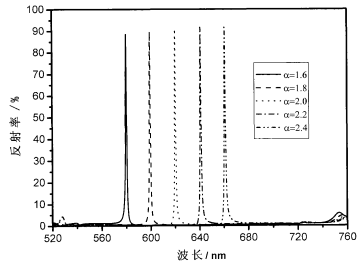

(c) Manipulation of α.

Fig. 9. Layout and Spectra Graphs for Single Peak Filter.
[26]

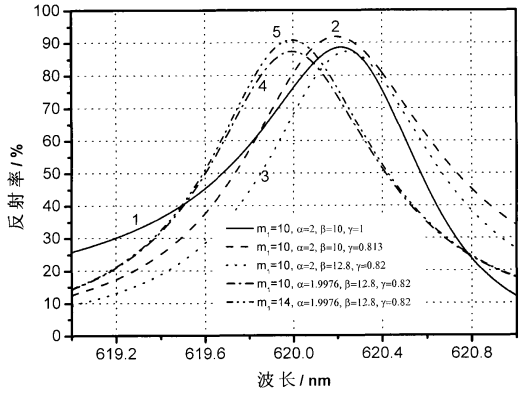

Fig. 10. Close Up of Spectra Graph of Single Peak Filter.

on the target pass wavelength, would promise a better and wider application in its use especially in astronomy and astrophotography. Lastly, it is important to note that while this design was submitted for the Chinese Patent, it was never passed after its submission in 2008. While its similarity to other patents might be the reason, we cannot also dismiss the possibility of its ineffectiveness or untruthfulness in its claims as being the cause.

3.2. Multiple peak narrowband reflection filter possessing broad low reflecting bypass belt

The Multiple Peak Narrowband Reflection Filter Possessing Broad Low Reflecting Bypass Belt [27] is a design submitted to the Chinese Patent office by the same inventor as the aforementioned product at approximately the same time. It details a photonic crystal narrowband filter structure design that is quite similar to the aforementioned Single Peak Narrowband design. It shares similarities in its basis for design (Asymmetric Fabry-Perot medium-metal construction), and the basic materials deployed. One main difference between the two designs is that the second design aims for the construction of multiples reflection peaks in the spectra graph with a more complex layering composition, compared with the simpler single peak design. The patent article states that this design allows for the number of the reflection peaks to be adjusted and controlled, as well as allowing the significant expansion of the low reflection bypass band. In line with the aforementioned single peak patent, this article also cites the two problems with the current existing product, and claims that this design is able to tackle both of them through the unique structure. It should be noted that, in contrast with the first design, this multiple peak narrowband design was passed and granted application by the Chinese patent office in December 22th, 2010.

The structure itself for this multiple peak design is $Sub|(HL)^{m1}H(\alpha 1LHLH)(\alpha 2LHLH)(\alpha qLHLH)L(HL)^{m2}\beta MP|Air$ as also shown in Figure 11a. The particular metal M here refers to the high-absorbing metal. More specifically, M can be tungsten, chromium, iron, nickel, lead, rhodium or other high-absorbing metal, such as Cr metal. H, L respectively are the high and low refractive index material of 1/4 wavelength optical thickness that is engineered such that it matches the target center wavelength. n_H and n_L are respectively the refractive index of high and low refractive index material. The present invention calculates n to be n_H=2.19, n_L=1.46. d_H, d_L respectively represents the physical thickness of two kind high low-index materials corresponding with 1/4 wavelength optical thickness. Sub represents the substrate of optical thin film, with refractive index taken as 1.52. Air represents air, with refractive index of 1. $m1$ and $m2$ are the repeating number of times of the corresponding (HL) layer, where $m1$ is greater than $m2$, and $m1$ is greater than 2, more than 10. $\alpha 1$, $\alpha 2$, and $\alpha 3$ are the thickness coefficient of the consequent L wall, and q is the integer number of the $(\alpha LHLH)$ repetitive. Just like the aforementioned single peak filter, two kinds of differing refractive index films can be used as the H layer of high refractive index, and L of low. Based on current developments, the combination of TiO_2 as high and SiO_2 as low is commonly used. These two kinds of differing dielectric constant films also can be the mantle based material, such as ZnS and MgF combination where it is the high material and low by order.

The film structure, as well as the value of each variable can be used to subtly manipulate the resulting spectra graph of the filter. The result of this manipulation and their multiple peak is also shown in Figure 11b and Figure 11c. $m1$ regulates and controls the height of the reflection peak, while $m2$ adjust the half width of narrowband reflection peak. The number of reflection peak is controlled by the thickness coefficient α of L wall 1. The position of reflection peak is changed by the thickness coefficient $\alpha 1$ and $\alpha 2$. Similarly, the width of low reflecting bypass belt and the degree of depth are adjusted by the appropriate combination of metal layer thickness β and admittance matching layer P. Pre-programmed computer processes can be used to optimize these parameters during the specific design engineering fine-tuning and obtain even more ideal spectral characteristics.

In sum, this design is able to produce a wide and low transmitting range, and a multiple peak reflection narrowband with a method for adjusting that reflective spectral property based on need. Furthermore, its regulation and control with reflection peak number can accurately control characteristics such as reflection peak width and position, and can be applicable in fields such as optical instrument, astronomy, remote sensing and optical communication. However, similar to the first single peak design, this product also has several notable problems. One is the low

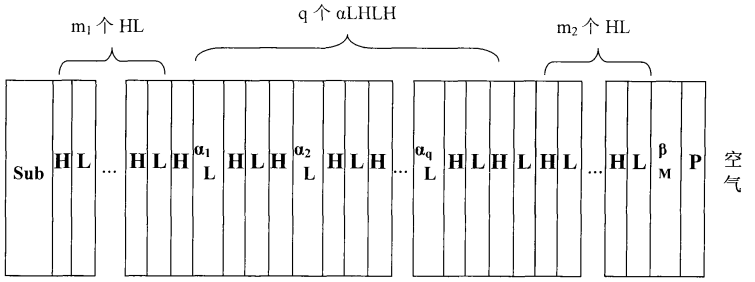

(a) Physical Layout.

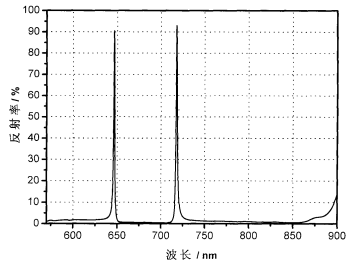

(b) 2 Reflection Peak.

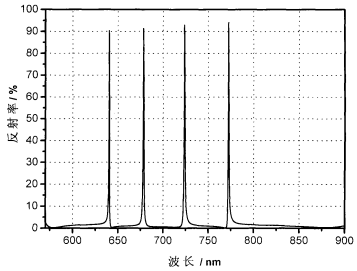

(c) 4 Reflection Peak.

Fig. 11. Layout and Spectra Graphs for Multiple Peak Filter.
[27]

transmittance rate of the peak reaching to only 90%, and the second is the inaccurate focus, as the bottom of the peak also includes significant percentage transmittance of the surrounding, non-intended wavelengths. Especially in the field of astronomy and the capture of photographs, this high transmittance rate and the acute focus is crucial for more accurate store and analysis. Finally, the overall structure of the design is very complex, and can produce problems and high cost in the actual manufacturing process. For a wider, more popular application in the real life field, a simpler and more effective design is needed.

4. Design

4.1. Overview of Hydrogen Alpha Target Design

Through utilizing the defect characteristic of photonic crystal, the research was successful in designing a thin film filter that only allows the transmittance of the targeted wavelength with the best possible efficiency and focus. The system of the filter consists of three 1-dimensional photonic crystal with soda lime glass substrate layer between. The total thickness of the filter was predicted to be approximately 9800 nms.

The first 1 dimensional Photonic crystal layer isolates the targeted wavelength in the range of approximately 567 to 780 nm. In this range, The transmittance rate of the target wavelength if 100 percent, while for almost every other wavelength excluding 2 additional peaks it is 0 percent as shown in Figure 12b. The band width of the peak or defect is less than 1 nm, approximately from 656 to 656.5 nm, also illustrated in 12c. The second layer consists of another photonic crystal that blocks every other wavelength of electromagnetic light outside of the 567 to 780 nm range. And finally, the third layer consists of another 1D photonic crystal that blocks from range 450 to 610 nm. All 3 layers plus the glass substrates will add up to about 9800 nms in total thickness.

The overall filter design ultimately yields a spectra (in the visible electromagnetic wave spectrum of 400 to 800 nm) with 100 percent transmittance rate at the targeted wavelength and 0 percent transmittance rate at almost every other wavelength as shown in Figure 16. The described filter design with specific numbers has the peak or defect in 656.279, the wavelength of Hydrogen Alpha. However, through the algorithm laid out below in Section 4.4 the location of the defect can be manipulated to other possible target wavelength of Hydrogen Beta and OIII.

This design is a significant improvement from any other nebula filters existing in the current market, and any other H-Alpha photonic crystal design from other researches. First and foremost, it yields 100 percent transmittance rate of the target wavelength, a feat no other design was able to achieve before. Secondly, at the same time it reaches its 100 percent rate, it is also able to focus the band width of the peak down to under 1 nm. This is a significant improvement from other designs that failed to attain both of these characteristics for the sake of achieving one or another. Lastly, the design is consisted of a relatively simple structure, when compared with similar researches done with 30+ layers as explained in Section 3. Both layers are 1D crystal structure, which implies that the production of the filter only require depositing the thin film layers onto a flat surface; no complex drilling or shaping process is needed for the filter's making. This signifies that this greatly simplifies the production process of the filter, and leads to a more promising possibility of being produced and used in real life.

4.2. Details of Structure

The photonic crystal for both layers were composed of 2 types of materials: TiO2 for high refractive index, and SiO2 for low refractive index. The exact value of refractive index used in the simulation code for TiO2 is 2.32. This is a value approximately by averaging out calculated refractive index values of the TiO2 thin film by 5 different studies. The details of the studies and its calculated value is as follows: 2.4335 from 2012 study by Kischkat et al. [28], 2.3361 from 2015 study by Zhukovsky et al. [29], 2.3364 from 2016 study by Siefke et al [30], 2.0916 from 2019 study by Sarkar et al. [31], 2.3667 from 2023 study by Jolivet et al [32]. The exact value of refractive index used in the simulation code for SiO2 is 1.46. This is a value approximated by averaging out calculated refractive index values of the SiO2 thin film by 4 different studies. The details of the studies and its calculated value is as follows: 1.4432 from 2012 study by Kischkat et al. [28], 1.4694 from 2013 study by Gao et al. [33], 1.4664 from 2013 study by Lemarchand [34], and 1.4580 from 2016 study by Rodríguez-de Marcos et al [35].

4.2.1. First Layer

The structure of the first layer which serves to primarily isolated the targeted H-alpha wavelength can be described by $(LH)^4/H/(LH)^{14}/H/(LH)^5$, where L denotes the layer of SiO2 and H layer of TiO2. The powers stands for the repetition of the layers inside the parenthesis. For instance, $(LH)^{14}$ indicates repetition of 14 times of the LH layers. The visualization of this one dimensional structure is showed by Figure 13. The thickness $d1$ of the SiO2 layer was $656.279/4/n1$ (with $n1$ being the refractive index of SiO2 used in this research) which calculated to 122.377 nm. The thickness $d2$ of the TiO2 layer was $656.279/4/n2$ (with $n2$ being the refractive index of TiO2 used in this research) which calculated to 70.720 nm. Furthermore, the reflectance, transmittance values and the spectra graph of this first photonic crystal layer was calculated through the TMM calculation method and code described in Section 2.

4.2.2. Second Layer

The second layer serves to block the resulting unnecessary side lobes by the first photonic crystal layer. It is a one dimensional photonic crystal structure with out any defects, with its layout simply being $(LH)^{15}$, or repetition of 15 times of the LH. The L and H in this notation still stands for the two materials used, SiO2 and TiO2 by the order. The lambda value for both layers

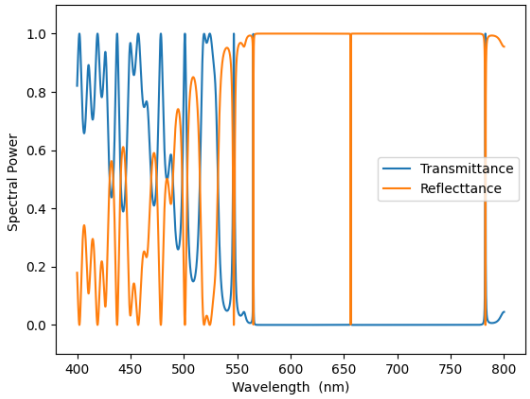

(a) Spectra Graph of First Layer in Visible Light Range.

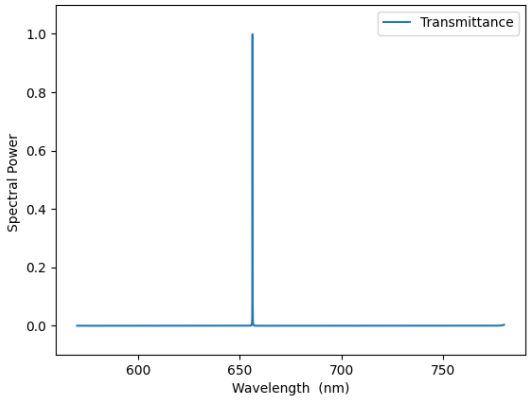

(b) Transmittance Spectra of First Layer from 560 to 790 nm.

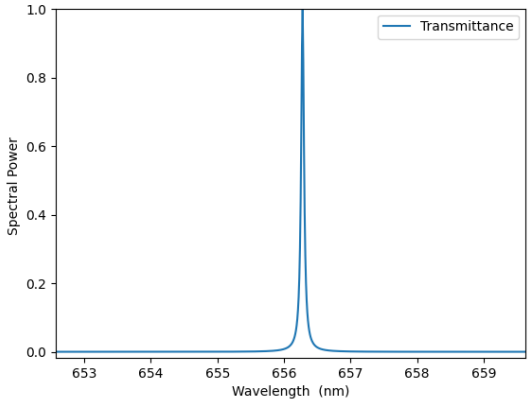

(c) Zoom in of Band Width of Defect.

Fig. 12. Spectra Graphs of First 1D Photonic Crystal Layer.

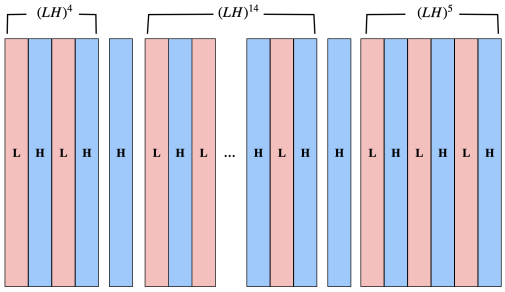

Fig. 13. Structure of First 1D Photonic Crystal Layer.

were 458.3, which resulted in the thickness 78.476 nm for the SiO2 layers ($d1$)and 49.386 nm for the TiO2 layers ($d2$). The resulting spectra graph had a photonic crystal band gap from approximately 400 nm to 540 nm, as seen in Figure 14a. Furthermore, its side lobes has been manipulated such that one lobe reached 100 percent transmittance rate at the exact targeted wavelength that the first layer isolated. For instance, from the zoomed in Figure 14b, that specific lobe reached 100 percent transmittance rate at wavelength about 656.3, which is the location of the peak wavelength. Thus, the second layer is able to minimize unnecessary noise with the blocking of the band gap, as well as still allowing the transmittance of the targeted wavelength.

4.2.3. Third Layer

The third layer serves the same purpose as the second layer: to block the unnecessary side lobes produced by the first layer while still allowing the transmittance of the targeted wavelength. It is a one dimensional photonic crystal structure with out any defects, with its layout simply being $(LH)^{14}$, or repetition of 14 times of the LH. The L and H in this notation still stands for the two materials used, SiO2 and TiO2 by the order. The lambda value for both layers were 522.8, which resulted in the thickness 89.52 nm for the SiO2 layers ($d1$)and 52.336 nm for the TiO2 layers ($d2$). The blocking range of the third layer is from approximately 450 to 610 nm, as shown in Figure 15a. Figure 15b shows that the lobe reached 100 percent transmittance rate at the targetted wavelength of 656.3 nm.

4.3. System of All Three Photonic Crystal With Substrate

Figure 16 illustrates the spectra graph of the entire system of all three photonic crystal layers. This system also includes a thick substrate layer between the photonic crystals such that the electromagnetic light working within the system of each photonic crystal is not interfered by the effects of other layers. The material of this substrate layer is soda lime glass, and its used refractive index is 1.5234. The order of the layers is as follows: Second layer (4.2.2), Third layer (4.2.3), an soda lime layer of thickness 1400 nms, and lastly the first layer 4.2.1. Whether or not the intermediate layer is air or soda lime glass has no notable effect on the resulting spectra graph, thus this section will only consider the system using the latter, which has more practical use. The whole system with the substrate results in a filter that can isolate the targeted wavelength at 656.3 with 97.9 percent transmittance. It is speculated that the multiple layering of the different photonic crystal layers resulted in a loss of 2.4 percent transmittance rate. The full width at half max of the peak is a mere 0.1 nm, demonstrating its improved focus on the targeted wavelength.

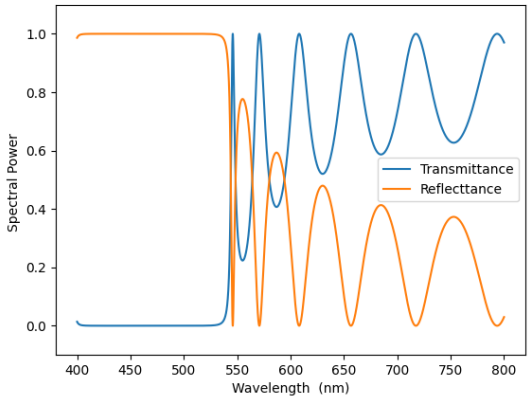

(a) Spectra Graph of Second Layer in Visible Light Range.

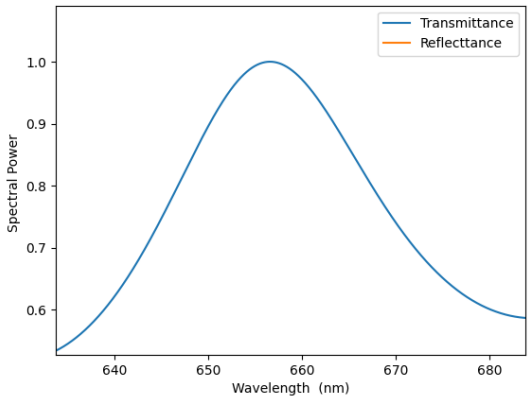

(b) Zoom into Lobe Allowing Targeted Wavelength.

Fig. 14. Spectral Graphs of Second 1D Photonic Crystal Layer.

4.4. Algorithmic Manipulation of Defect Wavelength

While the target wavelength in the aforementioned isolating filter in Section 4.2.1 is of Hydrogen Alpha (656.3), it is possible to change this wavelength using a algorithmic manipulation. The structural condition for the first isolating layer of 1D photonic crystal to produce the 100 percent transmittance peak as follows: $(LH)^a/H/(LH)^b/H/(LH)^c$, where the relationship between the number of repetition is $2c + a = b$. For instance, one set of numbers that satisfy this condition is $a = 2$, $b = 10$, $c = 4$, as $2 * 4 + 2 = 10$. The greater the number is for a, b, and c, the tighter the band width of the peak gets, however at the same time the other part of the spectra graphs becomes messier and fluctuating.

From the Figure 18 we can see that the greater the a, b, c values become, the more unnecessarily fluctuating the left portion of the spectra graph becomes. For the greatest a, b, c value of 5, 17, 6, respectively, even the peak on the intended Hydrogen Alpha wavelength decreased from the perfect 100 percent transmittance due to the over-repetition of the layers in the structure. Thus, it is crucial that we find the set of number that produces a balanced spectra graph appropriate for the appropriate wavelength. This algorithmic manipulation and relationship gives more potential

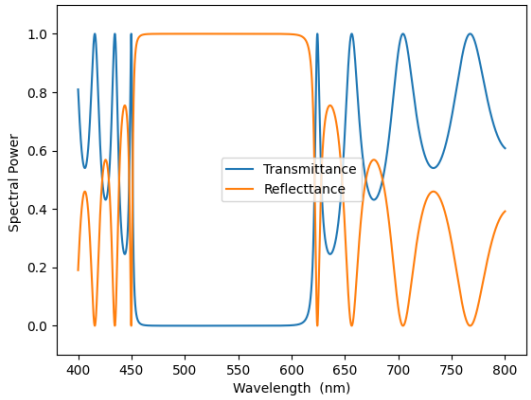

(a) Spectra Graph of Third Layer in Visible Light Range.

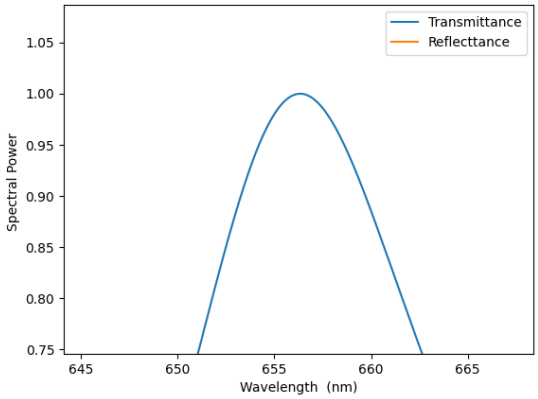

(b) Zoom into Lobe Allowing Targeted Wavelength.

Fig. 15. Spectral Graphs of Third 1D Photonic Crystal Layer.

for the design to be tailored to the different wavelengths intended to isolate and capture with the filter.

4.5. Consideration of Practical Manufacturing Factors

This short section is intended to acknowledge the elements and factors to consider during the real-life manufacturing process. For reference, a possible manufacture method of the photonic crystal layer of the filer is the Electron Beam Physical Vapor Deposition method. This EB-PVD technology [36] is a combination of electron beam technology and physical vapor technology, which uses high-energy-density electron beams to bombard targets (metals, ceramics, etc.) in a vacuum environment to evaporate them into atoms or molecules to form a vapor cloud. The vapor cloud is transported from the target source to the preheated processed substrate through a thin atmosphere, and the coating is formed by condensation deposition. For this specific filter, the two substrate that are evaporated into molecules to be deposited onto the surface are TiO2 and SiO2. The thickness of each layer would be manipulated through setting the time (minutes or seconds) that the molecule evaporation is allowed.

The first factor to consider is that while the spectra graphs of the filter referred in previous

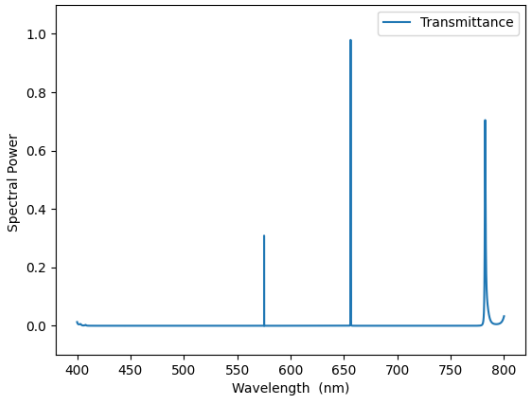

Fig. 16. Transmittance Spectra Graph of Whole System with All Three Layers and Substrate.

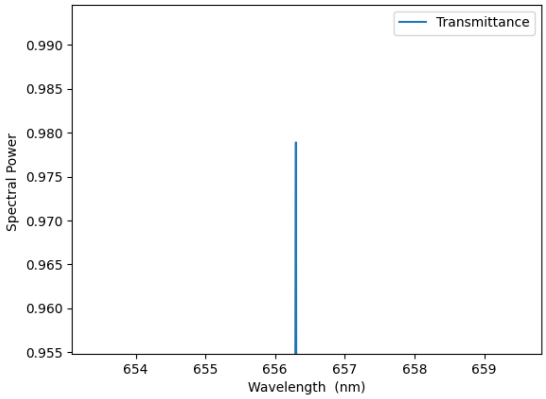

Fig. 17. Zoom into Peak.

Section 4 are created based on the model utilizing the refractive indices of average values from previous studies, in real-life manufacturing processes the refractive indices are actually calculated for the specific material used. Instead of taking the average values of several calculated refractive indices, during the manufacturing process the refractive index of the material to be used will be measure on the spot to be used and referred in later times. Thus, the minute difference that would rise between the average index value used in this study, and the actual measure value during production, must be considered in further manufactures or researches.

Secondly, it is critical to note that it would be a challenge in the manufacturing process to create a layer of air between the two layers of photonic crystal, especially if the process utilizes the EB-PVD method. Instead, a thin layer of soda lime glass substrate would be deposited between the different layers of photonic crystal, as also incorporated in 4.3. Soda-lime glass is the most common commercial glass that is comparatively inexpensive and amenable to recycling [37]. Clear soda lime glass has a refractive index of 1.5234, of internal transmittance rate (at thickness of 1 nm) reaching up to 1.000 [38]. Using a relatively thick soda lime substrate layer (compared to each TiO2 and SiO2 layers) between the different Photonic crystal will ensure that the reflection

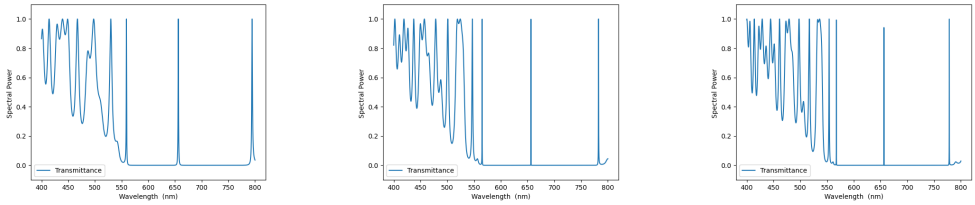

(a) a = 2, b = 10, c = 4. (b) a = 4, b = 14, c = 5. (c) a = 5, b = 17, c = 6.

Fig. 18. Comparison of Different Values for a, b, c.

within each photonic crystal will not interfere with the transmittance of other parts of the filter, and will not have any effect on the other spectra graphs. In the same line of reasoning, the individual spectra graphs of Figure 12 and Figure 14a are graphs created for the individual photonic crystal. There might arise minute difference for spectra graph when the whole system of several layers are taken as one photonic crystal. However, if we simply ensure that the glass substrate is thick enough to have no effect on the transmittance of other layers, it is very unlikely that there would be any significant difference. And it was also proven from the resulting spectra graph in previous sections that the substrate layer of soda lime glass has, in fact, no notable influence on the transmittance and reflection rates of the overall filter system.

The last element that should be considered is the first and last layer of the whole filter itself. Many of the existing and used filters have a thin layer of glass or protecting layer surrounding the actual functional filter layers to ensure that the filter is not scratched or effected by humidity. This is especially important for astrophotography filters, as they are used mostly at night, in an extremely cold or humid environment. Thus, consideration for this protection layer before the first photonic crystal and after the last one must be made and included in the final manufacturing design. However, the comparative thickness of these glass layers would ensure that it doesn't have any effect on the actual function of the filter, as also aforementioned for the glass substrate between the different photonic crystals.

5. Conclusion

This paper presented a novel H-Alpha filter design composed of 3 distinct photonic crystal layers with substrate disposed between. Utilizing the unique characteristics of photonic crystal band gap and defect mode, the filter was able to create a transmittance spectrum with a 97.9 percent rate in the targeted 656.3 H-Alpha wavelength while blocking almost every other wavelength of the visible light spectrum. The design was able to account for practical manufacturing components such as an simpler structure compared to other existing H-Alpha peak filter designs, and included the substrate layer between the photonic crystals for the method of EB-PVD to be used to dispose the material TiO2 and SiO2 vapors to be layered onto the surface. It presented the final spectrum graph created by the whole system of 3 photonic crystal and the glass layer which proved that adding the glass substrate instead of air had no notable effect on its transmittance rates if its thickness was significantly larger than that of individual layers of the photonic crystal. It also presented a algorithm or relationship between the repeating powers of the layers of the first isolating photonic crystal such the design can be applicable to not only H-Alpha wavelength but can be manipulated to isolate other wavelengths such as O3 and H-Beta. Its significance comes from the improvement it was able to make compared to the other existing H-Alpha filters. Firstly, it was able to achieve almost 100 percent transmittance rate of the isolated peak wavelength, compared to the usual 80 90 percent rate of the current market products. Secondly, coupled along with the high transmittance rate it has a extremely high focus of less than 1mn band width and

a full width at half max of 0.1mn. This is an unprecedented focus on the targeted wavelength, which is essential in the astrophotography and astronomy where the filters serve to capture only the wanted wavelength for clearer photographs of celestial bodies.

However, there are still improvements that can be made to the design in future works. One most significant shortcoming of this design is the two additional unnecessary peak created in the resulting spectra graph at approximately 570 and 790. While their transmittance rate are only respectively 30 and 70 percent, improvements can be made such that these peaks are not being transmitted at all by the filter. Increasing the thickness of the glass substrate between the isolating layer and the blocking layer might be a solution; however this thicker substrate layer has the side effects of lowering the transmittance rate of the main intended peak. Further research can be done to study the effects of the thickness of the substrate layer in both reducing the unintended peaks and also the transmittance rate of the targeted wavelength. Next, work can be done around double channel filters. While this specific design focused on single channel filters, which have only one targeted wavelength, a design that targets 2 or more wavelength to isolate is highly probable and has great application. For this case of astrophotography filter, one example would be a filter that isolate both H-Alpha and O3, which both are a big part of the electromagnetic lights emitted by nebulae.

Another component to consider is the unintended effects caused by the extremely narrow band width of the filter peak. As the allowed wavelength range is extremely narrow, a minute error caused during the manufacturing process might lead to the transmittance of wavelength other than the targeted one. Thus, one method to be considered is the calibration using the tilting of the photonic crystals. Light entering the photonic crystal tilted in an angle produces a spectrum that is shifted from the original. The location of the peak can thus be manipulated according by this calibration method to subtly adjust in case of manufacturing errors. Transfer Matrix Method calculation codes can be used to incorporate the factor of angle of incidence and predict the shift in the target peak in the spectrum.

Acknowledgments. I would like to give the warmest thanks to Professor Hossein Alisafaee for his guidance through the research, as well as the writing process. His detailed lessons and feedback was what made the work possible, pushing me forward into the right direction in every stage of the process.

References

1. S. Minardi, R. Harris, and L. Labadie, "Astrophotonics: astronomy and modern optics," The Astron. Astrophys. Rev. **29**, 1–81 (2021).
2. M. Middleton, P. Casella, P. Gandhi, E. Bozzo, G. Anderson, N. Degenaar, I. Donnarumma, G. Israel, C. Knigge, A. Lohfink *et al.*, "Paving the way to simultaneous multi-wavelength astronomy," New Astron. Rev. **79**, 26–48 (2017).
3. J. H. Kastner, D. A. Weintraub, I. Gatley, and L. Henn, "Kinematics of molecular hydrogen emission from pre-planetary nebulae: Rafgl 2688 and rafgl 618," The Astrophys. J. **546**, 279 (2001).
4. N. G. Douglas, M. Arnaboldi, K. Freeman, K. Kuijken, M. Merrifield, A. J. Romanowsky, K. Taylor, M. Capaccioli, T. Axelrod, R. Gilmozzi *et al.*, "The planetary nebula spectrograph: the green light for galaxy kinematics," Publ. Astron. Soc. Pac. **114**, 1234 (2002).
5. R. W. Pogge, J. M. Owen, and B. Atwood, "Imaging spectrophotometry of the orion nebula core. i-emission-line mapping and physical conditions," Astrophys. Journal, Part 1 (ISSN 0004-637X), vol. 399, no. 1, p. 147-158. **399**, 147–158 (1992).
6. A. Frankowski and N. Soker, "Very late thermal pulses influenced by accretion in planetary nebulae," New Astron. **14**, 654–658 (2009).
7. R. Lupu, K. France, and S. McCandliss, "Discovery of lyα-pumped molecular hydrogen emission in the planetary nebulae ngc 6853 and ngc 3132," The Astrophys. J. **644**, 981 (2006).
8. C. T. Corporation, "H-alpha 8nm bandpass," https://www.chroma.com/products/parts/h-alpha-8nm-bandpass (2023).
9. Vaonis, "Vespera dual band filter," https://vaonis.com/product/vespera-dual-band-filter (2023).
10. O. O. Co., "L-enhance eos-c clip filter for canon aps-c camera body," https://www.optolong.com/cms/document/detail/id/101.html (2023).
11. O. O. Co., "[2021 new] optolong sho-3nm narrowband filter," https://www.optolong.com/index.php/cms/document/detail/id/161.html (2021).

12. X. Lv, B. Zhong, Y. Huang, Z. Xing, H. Wang, W. Guo, X. Chang, and Z. Zhang, "Research progress in preparation and application of photonic crystals," Chin. J. Mech. Eng. **36**, 1–17 (2023).
13. G. von Freymann, V. Kitaev, B. V. Lotsch, and G. A. Ozin, "Bottom-up assembly of photonic crystals," Chem. Soc. Rev. **42**, 2528–2554 (2013).
14. E. Yablonovitch and K. Leung, "Photonic band structure: Non-spherical atoms in the face-centered-cubic case," Phys. B: Condens. Matter **175**, 81–86 (1991).
15. K. Ho, C. T. Chan, and C. M. Soukoulis, "Existence of a photonic gap in periodic dielectric structures," Phys. Rev. Lett. **65**, 3152 (1990).
16. Y. Xiong, S. Shepherd, J. Tibbs, A. Bacon, W. Liu, L. D. Akin, T. Ayupova, S. Bhaskar, and B. T. Cunningham, "Photonic crystal enhanced fluorescence: a review on design strategies and applications," Micromachines **14**, 668 (2023).
17. D. Gowdhami, V. Balaji, M. Murugan, S. Robinson, and G. Hegde, "Photonic crystal based biosensors: An overview," ISSS J. Micro Smart Syst. **11**, 147–167 (2022).
18. J. C. Corbett and J. R. Allington-Smith, "Coupling starlight into single-mode photonic crystal fiber using a field lens," Opt. Express **13**, 6527–6540 (2005).
19. J. Shao, G. Liu, and L. Zhou, "Biomimetic nanocoatings for structural coloration of textiles," in *Active coatings for smart textiles,* (Elsevier, 2016), pp. 269–299.
20. Y. Yue and J. P. Gong, "Tunable one-dimensional photonic crystals from soft materials," J. Photochem. Photobiol. C: Photochem. Rev. **23**, 45–67 (2015).
21. F. Dominec, C. Kadlec, H. Němec, P. Kužel, and F. Kadlec, "Transition between metamaterial and photonic-crystal behavior in arrays of dielectric rods," Opt. express **22**, 30492–30503 (2014).
22. M. Summers, K. Tabunshchyk, A. Kovalenko, and M. Brett, "Fabrication of 2d–3d photonic crystal heterostructures by glancing angle deposition," Photonics Nanostructures-Fundamentals Appl. **7**, 76–84 (2009).
23. M. Born and E. Wolf, *Principles of optics: electromagnetic theory of propagation, interference and diffraction of light* (Elsevier, 2013).
24. B. E. Saleh and M. C. Teich, *Fundamentals of photonics, Chapter 7: Optics of Dielectric Layered Media* (john Wiley & sons, 2019).
25. T.-C. King and C.-J. Wu, "Properties of defect modes in one-dimensional symmetric defective photonic crystals," Phys. E: Low-dimensional Syst. Nanostructures **69**, 39–46 (2015).
26. W. Yonggang, "Single peak narrowband reflection filter possessing broad low reflecting bypass belt," https://patentscope.wipo.int/search/en/detail.jsf?docId=CN83459929&_cid=P10-LLBNE6-86805-1 (2008).
27. W. Yonggang, "Multiple peak narrowband reflection filter possessing broad low reflecting bypass belt," https://patentscope.wipo.int/search/en/detail.jsf?docId=CN83459928&_cid=P10-LLBZYF-03744-1 (2008).
28. J. Kischkat, S. Peters, B. Gruska, M. Semtsiv, M. Chashnikova, M. Klinkmüller, O. Fedosenko, S. Machulik, A. Aleksandrova, G. Monastyrskyi *et al.*, "Mid-infrared optical properties of thin films of aluminum oxide, titanium dioxide, silicon dioxide, aluminum nitride, and silicon nitride," Appl. optics **51**, 6789–6798 (2012).
29. S. V. Zhukovsky, A. Andryieuski, O. Takayama, E. Shkondin, R. Malureanu, F. Jensen, and A. V. Lavrinenko, "Experimental demonstration of effective medium approximation breakdown in deeply subwavelength all-dielectric multilayers," Phys. Rev. Lett. **115**, 177402 (2015).
30. T. Siefke, S. Kroker, K. Pfeiffer, O. Puffky, K. Dietrich, D. Franta, I. Ohlídal, A. Szeghalmi, E.-B. Kley, and A. Tünnermann, "Materials pushing the application limits of wire grid polarizers further into the deep ultraviolet spectral range," Adv. Opt. Mater. **4**, 1780–1786 (2016).
31. S. Sarkar, V. Gupta, M. Kumar, J. Schubert, P. T. Probst, J. Joseph, and T. A. Konig, "Hybridized guided-mode resonances via colloidal plasmonic self-assembled grating," ACS applied materials & interfaces **11**, 13752–13760 (2019).
32. A. Jolivet, C. Labbé, C. Frilay, O. Debieu, P. Marie, B. Horcholle, F. Lemarié, X. Portier, C. Grygiel, S. Duprey *et al.*, "Structural, optical, and electrical properties of tio2 thin films deposited by ald: Impact of the substrate, the deposited thickness and the deposition temperature," Appl. Surf. Sci. **608**, 155214 (2023).
33. L. Gao, F. Lemarchand, and M. Lequime, "Refractive index determination of sio2 layer in the uv/vis/nir range: spectrophotometric reverse engineering on single and bi-layer designs," J. Eur. Opt. Soc. publications **8** (2013).
34. L. Gao, F. Lemarchand, and M. Lequime, "Exploitation of multiple incidences spectrometric measurements for thin film reverse engineering," Opt. express **20**, 15734–15751 (2012).
35. L. V. Rodríguez-de Marcos, J. I. Larruquert, J. A. Méndez, and J. A. Aznárez, "Self-consistent optical constants of sio 2 and ta 2 o 5 films," Opt. Mater. Express **6**, 3622–3637 (2016).
36. H. Guo, Y. Guo, Z. Xue, S. Gong, and H. Xu, "Overview of thermal barrier coatings for advanced gas turbine engine," in *Thermal Barrier Coatings,* (Elsevier, 2023), pp. 1–20.
37. J. G. R. Sereni, "Reference module in materials science and materials engineering," (2016).
38. M. Rubin, "Optical properties of soda lime silica glasses," Sol. energy materials **12**, 275–288 (1985).